Experiments in Fluids 34 (2003) 140–149
DOI 10.1007/s00348-002-0546-0

Mean flow and turbulence measurements of the impingement wall jet on a semi-circular convex surface

T.L. Chan, Y. Zhou, M.H. Liu, C.W. Leung

Abstract The detailed mean flow and turbulence measurements of a turbulent air slot jet impinging on two different semi-circular convex surfaces were investigated in both free jet and impingement wall jet regions at a jet Reynolds number Re_w=12,000, using a hot-wire X-probe anemometer. The parametric effects of dimensionless circumferential distance, S/W=2.79–7.74, slot jet-to-impingement surface distance Y/W=1–13, and surface curvature D/W=10.7 and 16 on the impingement wall jet flow development along a semi-circular convex surface were examined. The results show that the effect of surface curvature D/W increases with increasing S/W. Compared with transverse Reynolds normal stress, $\overline{v^2}/U_m^2$, the streamwise Reynolds normal stress, $\overline{u^2}/U_m^2$, is strongly affected by the examined dimensionless parameters of D/W, Y/W and S/W in the near-wall region. It is also evidenced that the Reynolds shear stress, $-\overline{uv}/U_m^2$ is much more sensitive to surface curvature, D/W.

List of symbols

D	diameter of a semi-cylinder
L	slot length at nozzle exit
P	production term of turbulence energy
P_u	production rate of $\overline{u^2}/2$
P_v	production rate of $\overline{v^2}/2$
P_{uv}	production rate of $\overline{uv}$
q^2	turbulence energy, $q^2 = \overline{u^2} + \overline{v^2} + \overline{w^2}$
Re_w	Reynolds number based on nozzle width, $Re_w = \frac{U_e W}{\nu}$
R	radius of a semi-cylinder
S	circumferential distance along the semi-cylinder surface from the stagnation line, $S=\theta\times R$
u, v	turbulence velocities in x and y directions
U,V	mean velocity components in x and y directions
U_e	mean velocity at slot nozzle exit
U_c	streamwise mean velocity along the centreline of a free slot jet
U_f	skin friction velocity
U_m	maximum velocity across impingement wall jet
W	slot width at nozzle exit
x, y, z	spatial coordinate system
$y_{1/2}$	half width of impingement wall jet, where $U=U_m/2$ in jet region
y_m	radial location where the streamwise Reynolds normal stress is maximum
y_o	radial location where the Reynolds shear stress is zero
Y	slot jet-to-impingement surface distance
θ	angular position measured from stagnation line
ν	air kinematic viscosity
$\bar{}$	time averaging

Received: 11 June 2001 / Accepted: 30 August 2002
Published online: 19 October 2002

T.L. Chan (✉), Y. Zhou, C.W. Leung
Department of Mechanical Engineering,
The Hong Kong Polytechnic University,
Hung Hom, Kowloon, Hong Kong
E-mail: mmtlchan@inet.polyu.edu.hk
Tel.: +852-2766-6656
Fax: +852-2365-4703

M.H. Liu
Department of Thermal Science and Energy Engineering,
The University of Science and Technology of China,
Hefei, Anhui, China

The authors would like to thank The Hong Kong Polytechnic University for financial support (Project No. PB31) for this work. A vote of thanks is also extended to Prof. K. Jambunathan and Dr. S. Ashforth-Frost from The Nottingham Trent University, UK, for their advice in developing the jet impingement research work through the British Council funding which helped to strengthen research collaboration between the two universities in the early stages.

1 Introduction

Impingement jets are widely used for heating, cooling and drying operations because of their excellent convective heat and mass transfer rates. They also permit the simultaneous attainment of different flow regions in which the applications are different. A number of critical reviews and bibliographical forms on flow and heat transfer under impinging jets have been published by Martin (1977), Hrycak (1981), Launder and Rodi (1981), Downs and James (1987), Jambunathan et al. (1992), Viskanta (1993) and Chan et al. (1999a, 1999b). These reviews highlight the paucity of information on the turbulence characteristics of jets impinging onto a curved surface. Even the early researchers such as Gardon and Akfirat (1965) highlighted the importance of hydrodynamics effects along the curved surface. In fact, the study of the turbulent impingement wall jet can provide a better understanding of the surface curvature effect on the hydrodynamic processes associated with the heat transfer mechanism. However, it is important to understand the surface curvature effects not only on the mean flow characteristics but also on the turbulent

impingement wall jet structure and the momentum transport along the curved surface.

Many industrial curved applications include, for example, the heating, cooling and/or drying of painted cylinders, glasses, gas turbine parts, papers, textiles, film materials, foodstuffs, age hardening, the de-icing of aircraft wings, etc. Despite the industrial relevance of jet impingement on a circular convex surface, the surface curvature effects on the impingement wall jet flow structure are not yet well understood. The wall jet is used in most practical applications to control the boundary layer to heat or cool the solid surface and is in a turbulent state, although a two-dimensional wall jet generated by a slot nozzle placed tangentially on mildly, moderately and strongly curved surfaces was well studied by Gibson et al. (1984), Kobayashi and Fujisawa (1983) and Fujisawa and Kobayashi (1987). Similar wall jets over a convex surface were also studied by Alcarza et al. (1976) and Wilson and Goldstein (1976), while Neuendorf and Wygnanski (1999) studied the effect of surface curvature on the development of a two-dimensional wall jet around a circular cylinder. The wall jet of slot jet impingement on a wedge was investigated by Yamada et al. (1990) and Faruque et al. (1992). Recently, the effect of longitudinal curvature and transverse curvature on the turbulent boundary have been well summarised by Patel and Sotiropoulos (1997) and Piquet and Patel (1999) respectively. In fact, the flow of a fully developed turbulent impingement wall jet consists of two regions, namely the jet region and the wall region. These two regions were combined with each other continuously and interfered everywhere within the region where the velocity was maximum. The mean flow characteristics of slot jet impingement on a cylinder were studied by Barahma et al. (1991). In one of the more recent studies, Lee et al. (1997) investigated the effects of hemispherically convex surface curvature on the flow and heat transfer from a fully developed axisymmetric impinging jet. During slot jet impingement onto a cylinder surface, the wall jet is developed along the curved surface in which the surface curvature effects on hydrodynamic and heat transfer processes have been shown to be significant by Gau and Chung (1991) and Yang et al. (1999). Choi et al. (2000) studied the jet impingement flow and heat transfer on a semi-circular concave surface. They correlated the occurrence and location of the secondary peak of heat transfer data with measured mean velocity and velocity fluctuations on the concave surface. Liu et al. (2000) investigated the flow development of a turbulent slot jet impinging on a semi-cylindrical convex surface.

The aim of the present work is to provide the quantitative mean flow and turbulence measurement data of the impingement wall jet region associated with its near-wall velocity and turbulence properties on a semi-circular convex surface due to the parametric effects of the dimensionless circumferential distance, S/W, the slot nozzle-to-impingement surface distance, Y/W, and the surface curvature, D/W, for a fixed jet Reynolds number, Re_w. The data can also serve as bench-mark data for validating and refining turbulence models for the impingement wall jet flow development on a curved surface.

2
Flow regions description

A typical air slot jet impinging on a semi-circular convex surface is shown in Fig. 1. The flow structure of a slot jet impinging on a semi-circular convex surface can be subdivided into three distinctive regions: the free jet region, the impingement (deflection) flow region, and the wall jet region.

According to the description of Viskanta (1993), in the free jet region, the shear-driven interaction of the exiting jet and the ambient produces an entrainment of mass, momentum and energy. These combined effects introduce the development of a non-uniform radial velocity profile, expansion of the jet, an increase in total mass flow rate, and modification of the jet temperature before it impinges upon the target surface. The free jet region can be further subdivided into flow establishment and established flow zones. In the flow establishment zone, the velocity remains constant in the potential core and equals the nozzle exit velocity, whereas the length of the potential core is strongly dependent on the turbulence intensity of the nozzle exit and its initial velocity profile. The established flow zone is characterised by the decay of the axial velocity profile, resulting in large shear stresses at the jet boundary. Due to these large shear stress effects, turbulence and the entrainment of additional fluid were promoted and generated. After the established flow zone, the velocity profile was considered fully developed. The impingement zone is characterised by a deflection region and the turning of the jet fluid in the circumferential and radial directions, which affects the wall jet transition further downstream. The thickness of the impingement zone boundary layer is approximately constant. In the stagnation region, the flow is deflected in the circumferential direction. The flow decelerates sharply, followed by acceleration in the circumferential direction. The flow develops into a wall jet. The wall jet region is characterised by a bulk fluid flow in the outward circumferential direction.

3
Experimental details

The system consists of the air supply system, traverse and ancillary equipment. To ensure high air quality, air from the compressed air line passed through an air filtering system, a refrigerated air dryer, a high precision regulator, an air receiver tank, and then through a settling chamber and contraction containing a layer of aluminium honeycomb. This was in order to straighten the flow- and turbulence-reducing screens to produce a uniform velocity profile at the nozzle outlet. The contraction to the slot nozzles was designed as suggested by Button and Leech (1972). The contraction length and the nozzle curvature were calculated in such a way as to minimise the growth of the boundary layer. The high-precision slot nozzle had a smooth curvature made by the Deckel milling numerical control machine with calculated contraction values, which allows rapid acceleration of air without the occurrence of flow separation and generation of turbulence. A slot nozzle of width W 9.38 mm, and length L 125 mm was used. The aspect ratio of the slot jet enabled the flow to be considered two-dimensional at the centre of the slot exit plane, as described by Ashforth-Frost et al. (1997).

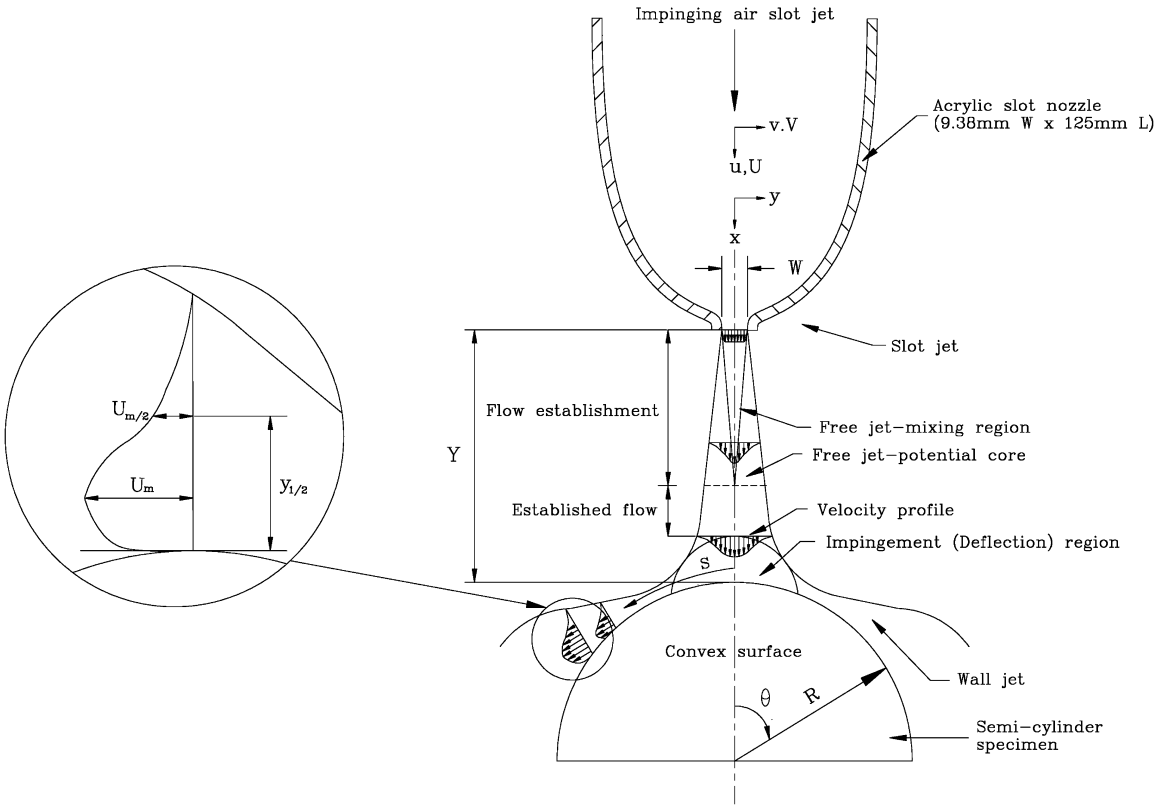

Fig. 1. A typical air slot jet impinging on a semi-circular convex surface

Two acrylic semi-cylinders of diameters D=100 mm and 150 mm (i.e. the surface curvatures D/W=10.7 and 16) were used as the impingement convex surface. The semi-cylinder was fixed on a tailor-made traverse mechanism so that the slot jet-to-impingement surface distance, Y, could be adjusted. Measurements were conducted from the dimensionless slot nozzle-to-impingement surface distances, Y/W=1–13 for the free-jet region, while Y/W=5 to 13 for the wall jet region at the selected dimensionless slot jet-to-circumferential distances, S/W=2.79, 4.19, 5.58 and 7.74 for both regions. The selected circumferential distances S corresponded to the semi-circular convex angle θ=30°, 45°, 60° and 80° for the semi-cylinder diameter D=100 mm, while θ=20°, 30°, 40° and 53.3° for the semi-cylinder diameter D=150 mm respectively.

A custom-made hot-wire X probe with a spatial resolution of about 1.0 mm was used to measure mean flow and turbulence data in the streamwise and widthwise directions u and v respectively. The wires were etched from a 5-μm diameter Wollaston (Pt–10% Rh) wire to a length of about 1 mm, leading to a ratio of about 200 for its hot-wire length and diameter. A constant-temperature circuit was used for the operation of the hot wires. An overheat ratio of 0.8 was used for the X-wire. Signals from the circuits were offset, amplified and then digitised using a 16-channel (12-bit) A/D board and a personal computer at a sampling frequency of 3.5 kHz per channel. The duration of each record was about 15 s. In order to obtain mean flow and turbulence data of good quality, the plane of the X-wire was placed parallel to the impingement surface at the nearest 0.1 mm from the surface with the step increment of 0.01 mm. Hence, no wall effects were evident in the X-wire data. Although the effect of the mean velocity gradient along the length of a single hot-wire might occur, the error could be less than 1.5% for both the mean flow and turbulence data if the ratio of hot-wire length to diameter was about 200, as described by Talamelli (2000). In addition, there was no temperature gradient along the hot-wire. There was no temperature difference between the in-situ X-wire calibration and the experimental measurements. Furthermore, the X-wire was under the same velocity profile, in which there was no shear between the displacement of the two wires at about 1 mm. The hot-wire X probe was calibrated using the same technique for turbulent flow measurement as suggested by Browne (1989). In the present study, the uncertainty in mean flow velocity was estimated to be within 1.7% using the hot-wire X probe as described by Holman (1978). According to the random theory of Bendat and Piersol (1986), the uncertainty of $\sqrt{\overline{u^2}}$, $\sqrt{\overline{v^2}}$ and $\overline{uv}$ was estimated to be within 4.5%, 5.3% and 12.5%, respectively. Details on the validation of using a hot-wire X probe anemometer for the present mean flow and turbulence measurements can also be found in the recent work of Zhou et al. (2000), Liu et al. (2000) and Chan et al. (2002).

4
Results and discussion

4.1
Free jet region

A uniform velocity profile associated with relatively low turbulence intensity across the slot nozzle exit was

measured. The streamwise turbulent intensity was found to be less than 0.9% across the width of the slot nozzle exit for the studied jet Reynolds number, Re_w=12,000. Similarly, the slot jet exit velocity and turbulence intensity profiles were reported in Ashforth-Frost et al. (1997). Figure 2 shows the typical symmetrical normalised mean velocities, U/U_m, streamwise and widthwise Reynolds normal stresses, $\overline{u^2}/U_m^2$ and $\overline{v^2}/U_m^2$ respectively, and the Reynolds shear stress, $-\overline{uv}/U_m^2$ for a free air jet at the centre of the slot exit plane ranging from Y/W=1–13. The Reynolds normal stresses show two peaks near the slot nozzle edge at y/W=±0.5, due to mixing in the turbulent shear layers where large velocity gradients exist. As Y/W increases, the mixing layer expanding causes the maximum turbulence intensity to move away from the jet centreline. The magnitude of the streamwise Reynolds normal stress $\overline{u^2}/U_m^2$ reaches the maximum level at about 0.0293 (the circumferential turbulence intensity, $\sqrt{\overline{u^2}}/U_m$=17.1%) when Y/W=7 to 9 and y/W=±0.8, but it becomes much broader and decreases rapidly when Y/W>9 as shown in Fig. 2b. However, the maximum widthwise Reynolds normal stress, $\overline{v^2}/U_m^2$ is about 0.0235 at Y/W=3 and y/W=±0.6, as shown in Fig. 2c. Two peaks of widthwise Reynolds normal stress across the slot jet appear for Y/W<13 and disappear for Y/W≥13. This means that the mixing rate in the widthwise direction is faster than that in the streamwise direction. When the mean velocity reaches its maximum, the Reynolds shear stress is zero, as shown in Fig. 2d. The maximum Reynolds shear stress occurs at about Y/W=7. As Y/W increases, the maximum shear stress moves away from the free jet centreline due to the expanding mixing layer. Figure 3a shows that the jet potential core ended at Y/W=4.6, based on the streamwise mean velocity, U_c=0.95U_e. Martin (1977) noted that the free slot jet has a potential core of approximately four slot widths, although a wider range was also found by other investigators. Livingood and Hrycak (1973) reported that the potential core extended 4.7–7.7 slot nozzle widths from the nozzle exit for a slot jet. Similarly, the slot jet potential core of approximately six slot widths was also found in Chan et al. (2002). Figure 3 shows the axial variations Y/W of developing jet flow structure from the normalised mean velocity and Reynolds normal stresses distributions along the jet centreline for Re_w=12,000. Mean velocities at the slot nozzle exit are maintained for certain distances within the potential core region, then decrease in different ways, depending on Reynolds numbers and nozzle widths. The penetration of the shear effect can carry the air in the jet centreline farther downstream due to the uniform velocity at the nozzle exit. Streamwise turbulence intensity along the free jet centreline increases sharply before reaching its maximum value, which occurs near Y/W=8.5, as shown in Fig. 3b. It is also found that the streamwise Reynolds normal stress reaches its maximum value at an earlier Y/W location than the widthwise Reynolds normal stress. This means that streamwise Reynolds normal stress is more sensitive to the expanding of the mixing layer along the free jet centreline.

4.2
Impingement wall jet region

If the transition flow takes place following the impingement of a jet, the jet must be a laminar one, as described by Vickers (1959) or the jet potential core just touches the impingement surface as described by Ashforth-Frost et al. (1997). In order to avoid the transition flow taking place on the impingement wall jet, the length of the potential core of a free slot jet was investigated to ensure that the jet was the fully developed turbulent one. In Fig. 3a, the jet potential core for Re_w=12,000 was found to end at around Y/W=4.6. Hence, the mean flow and turbulence measurements of the impingement wall jet on a semi-circular convex surface were investigated to the nearest axial slot jet-to-impingement surface distance, starting from Y/W=5

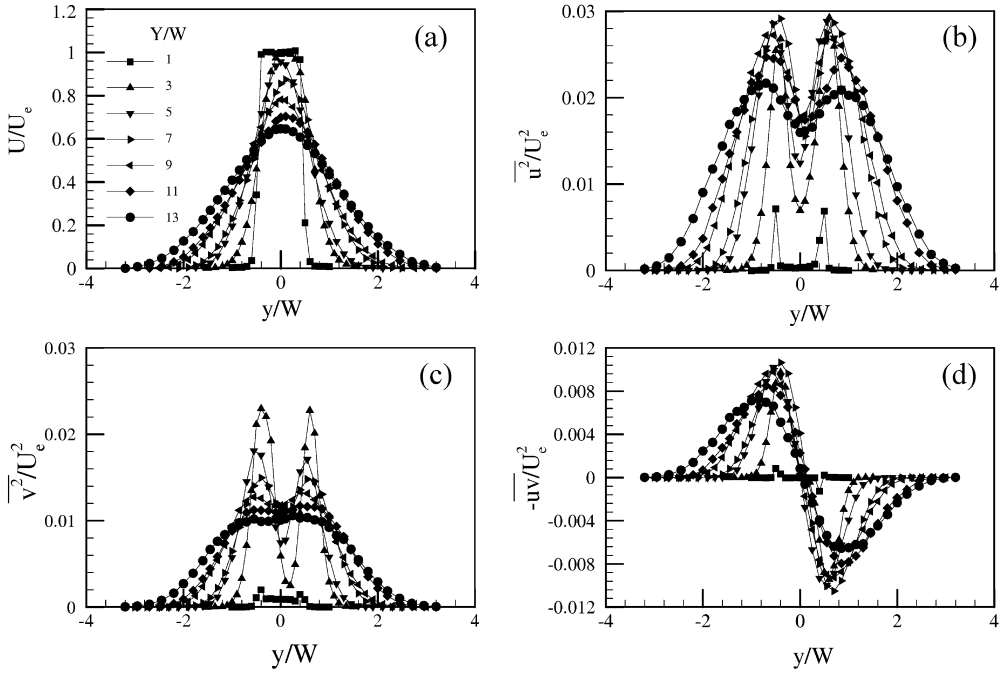

Fig. 2. Free slot jet measurements (W=9.38 mm, Re_w=12,000)

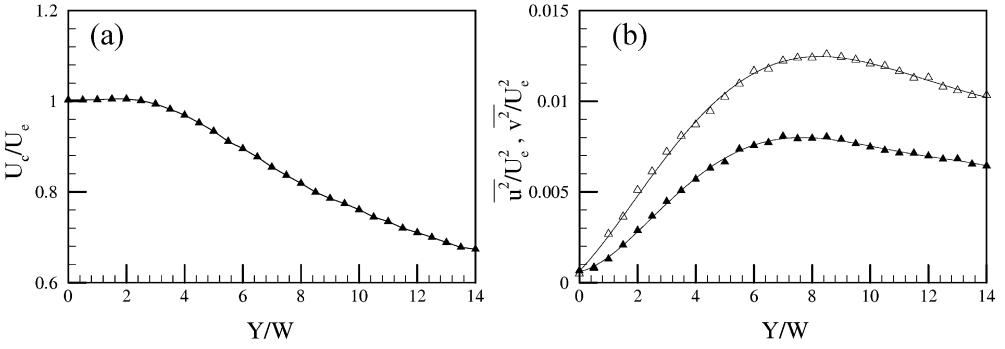

Fig. 3. **a** Mean velocity and **b** streamwise (*hollow symbols*) and widthwise (*filled symbols*) Reynolds normal stresses profiles along the free jet centreline (W=9.38 mm, Re_w=12,000)

to 11 for the present study. The mean velocity and the Reynolds normal and shear stresses across the wall jet at the circumferential locations of S/W=2.79, 4.19, 5.58 and 7.44 for both semi-cylinders, D/W=10.7 and 16, are shown in Figs. 4 and 5. The results are normalised by the same local maximum velocity, U_m and the half-width of the jet, $y/y_{1/2}$. In the wall jet region measured, the normalised mean velocities at different S/W coincide reasonably well, as shown in Figs. 4a and 5a. This is due to the constant surface pressure or self-similarity of the mean flow region as described by Neuendorf and Wygnanski (1999). With increasing S/W, the maximum points of the normalised streamwise and radial turbulence intensities increase accordingly, as shown in Figs. 4b, c and 5b, c. This is due to the interference between the wall region and the jet region within the region where the velocity is maximum. The streamwise Reynolds normal stress $\overline{u^2}/U_m^2$ distribution shows a single peak alone in Figs. 4b and 5b. However, Neuendorf and Wygnanski (1999) found that Reynolds normal stress is characterised by two high-intensity regions. In their study of a turbulent wall jet (nozzle placed on the wall tangentially) flowing over a circular cylinder, $\overline{u^2}/U_m^2$ was identified with two distinct regions. One was located in the outer part of the flow at around $y/y_{1/2}$=0.7, and the other near the surface at $0.02<y/y_{1/2}<0.04$: these locations depend on the direction of streamline. However, the high-intensity region near the surface is non-existent at the angular position, θ=40°. As θ or S/W increases, $\overline{u^2}/U_m^2$ increases and exceeds the maximum intensity measured in the plane wall jet by 64% at around θ=200°. In the present study, the maximum measured angular location for the semi-circular convex surface is less than 90°, hence it might lead to no double peaks in the $\overline{u^2}/U_m^2$ distribution.

The streamwise Reynolds normal stress, $\overline{u^2}/U_m^2$ increases with the increase in S/W as indicated in Figs. 4b and 5b. The magnitude increases significantly in the region of $y/y_{1/2}<1.2$, due to interference between the wall and jet regions of the wall jet. The radial location, y_m, where $\overline{u^2}/U_m^2$ is maximum, decreases as S/W increases. This is consistent with the findings of Neuendorf and Wygnanski (1999). The radial locations of $y_m/y_{1/2}$=0.88 at S/W=2.79 and $y_m/y_{1/2}$=0.54 at S/W=7.74 were found for D/W=10.7. However, the radial locations of $y_m/y_{1/2}$=0.92 at S/W=2.79 and $y_m/y_{1/2}$=0.56 at S/W=7.74 were found for D/W=16. Hence, this implies that the surface curvature affects the jet flow structure for the same selected range of S/W at y_m where the local $\overline{u^2}/U_m^2$ reaches its maximum value. The magnitude of

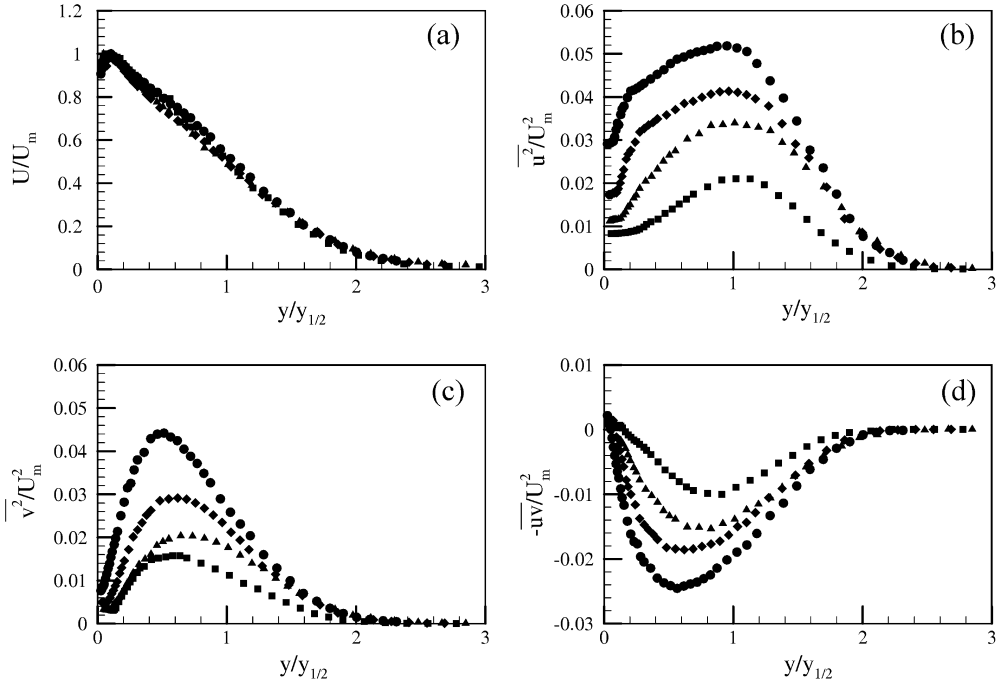

Fig. 4. Normalised mean velocity, Reynolds normal and shear stresses profiles across the impingement wall jet at different dimensionless circumferential distances, S/W: *filled squares*, 2.79; *filled triangles*, 4.19; *filled diamonds*, 5.58; *filled circles*, 7.74 (W=9.38 mm, Re_w=12,000, Y/W=9, D/W=10.7)

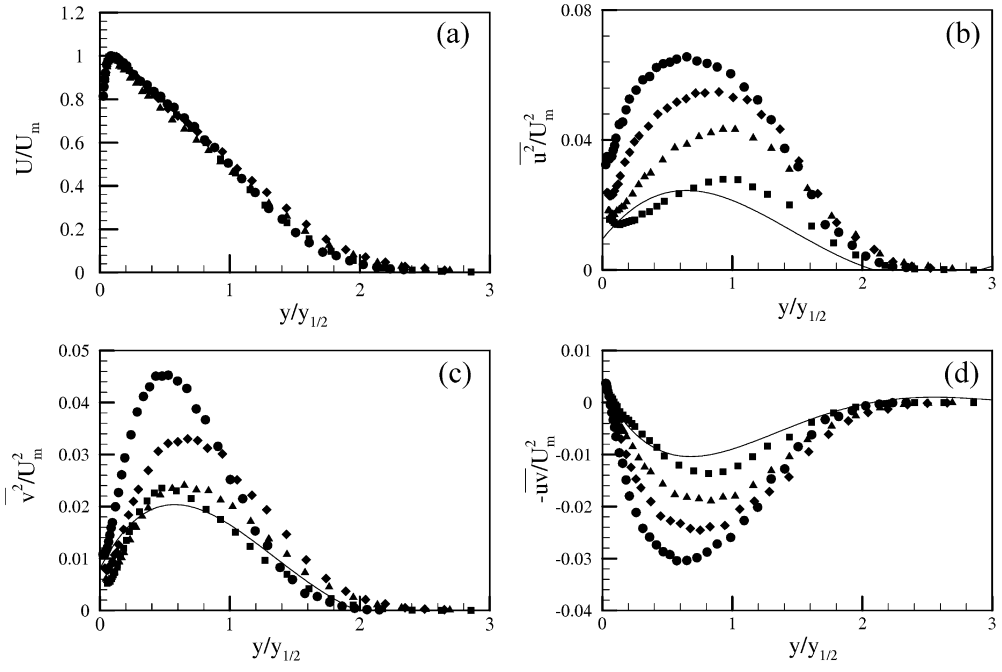

Fig. 5. Normalised mean velocity, Reynolds normal and shear stresses profiles across the impingement wall jet at different dimensionless circumferential distances, *S*/*W*: *filled squares*, 2.79; *filled triangles*, 4.19; *filled diamonds*, 5.58; *filled circles*, 7.74; *line*, Gibson et al. (1984) (W=9.38 mm, Re_w=12,000, Y/W=9, D/W=16)

transverse Reynolds normal stress, $\overline{v^2}/U_m^2$ in respect of $y/y_{1/2}$ reaches its maximum value, which also increases as *S*/*W* increases from 4.19 to 7.74 as shown in Figs. 4c and 5c. However, the maximum value of $\overline{v^2}/U_m^2$ at S/W=2.62 is slightly closer to the wall surface, due to the nozzle jet deflection. The magnitude of $\overline{v^2}/U_m^2$ doubles over the range of $2.79 \le S/W \le 7.74$ for both semi-cylinders.

By examining the shape of the distributions, it is found that $\overline{u^2}/U_m^2$ increases strongly near to the wall surface, but $\overline{v^2}/U_m^2$ increases to a lesser extent when *S*/*W* approaches the stagnation point, S/W=0. The difference in $\overline{v^2}/U_m^2$ between S/W=2.79 and 4.19 is much smaller than that of $\overline{u^2}/U_m^2$, as shown in Figs. 4b, c and 5b, c. For a small *S*/*W* range, $\overline{u^2}/U_m^2$ and $-\overline{uv}/U_m^2$ increase significantly, while $\overline{v^2}/U_m^2$ is less affected due to the strong wall damping effect. It is expected that the y location where $-\overline{uv}/U_m^2$ attains its maximum value will also decrease relative to $y_{1/2}$ with the increase in *S*/*W* as shown in Figs. 4d and 5d. The maximum value of $-\overline{uv}/U_m^2$ increases as the *S*/*W* increases. In the range of $2.79 \le S/W \le 7.74$, the magnitudes of $\overline{u^2}/U_m^2$, $\overline{v^2}/U_m^2$ and $\overline{uv}/U_m^2$ increase by a factor of 2.53, 2.72 and 2.5 for D/W=10.7, and 2.69, 1.88 and 3.01 for D=16 as shown in Figs. 4 and 5 respectively. However, U_m decreases by a factor of 1.45 in the selected *S*/*W* range. The ratio $\left(\sqrt{\overline{u^2}}/\sqrt{\overline{v^2}}\right)_{max}$ increases from 1.04 at S/W=2.74 to 1.21 at S/W=7.74. The maximum of $\overline{uv}/\sqrt{\overline{u^2}}\sqrt{\overline{v^2}}$ exceeds 0.52, which is larger than that of the plane wall jet case (0.49) and significantly larger than that in the turbulent boundary layer over a flat plate as shown in Fig. 6. The radial location of $y/y_{1/2}$, where $\overline{uv}/\sqrt{\overline{u^2}}\sqrt{\overline{v^2}}$ attains its maximum value, does not increase significantly with *S*/*W*. Neuendorf and Wygnanski (1999) found that $y/y_{1/2}$ changed from 0.5 at θ=40° to 1 at θ=200°. They described these observations as being peculiar to a wall jet placed on the surface. Based on their results, it can be concluded that the surface curvature and associated centrifugal force might alter the turbulent flow structure.

One of the significant features for turbulent wall jets, the location where the Reynolds shear stress becomes zero, does not agree with the location of the maximum velocity, which is in contrast to other shear flows such as pipe flows and free jet cases at y_o/y_m. This phenomenon is also found in the present study.

4.2.1
Surface curvature effect

Usually, the surface curvature D/W effect on flow behaviour can be compared with the plane and curved (i.e. concave and convex) surface. The studied angular position is less than θ=80° and 53.3° for D/W=10.7 and 16 respectively. Hence, it is reasonable to assume that the longitudinal pressure gradient in the boundary layer is negligible, as suggested by Neuendorf and Wygnanski (1999). The flow structure difference in the impingement wall jet between two semi-cylinders at the same Y/W, *S*/*W* and Re_w can be largely attributed to the surface curvature effect. These effects are quite significant, as evidenced in Figs. 7, 8 and 9.

In the study on the turbulent wall jet, the primary interests are the wall shear stress or skin friction, τ_w, the growth rate of the outer layer, and the mean flow velocities and Reynolds stresses across the wall jet. Two kinds of scales for the inner wall and outer jet regions were normally used in past investigations. For the inner wall region, the length and velocity scales are y_m (i.e. the value of y at U_m) and U_f respectively. For the outer jet region, the length and velocity scales are $y_{1/2}$ (i.e. the value of y at $U=U_{m/2}$) and U_m. Based on the present measurement technique, the jet length and velocity scales used are $y_{1/2}$ and U_m respectively.

The effect of streamwise curvature on mean velocity and Reynolds normal stress for different *S*/*W* ranges from 2.79 to 7.74 is shown in Fig. 7. For the slot nozzle used, the nozzle jet at Y/W=7 is well developed, as shown in Fig. 3. At individual *S*/*W* locations, the normalised mean velocity coincides reasonably well from S/W=2.79 to 7.74. The

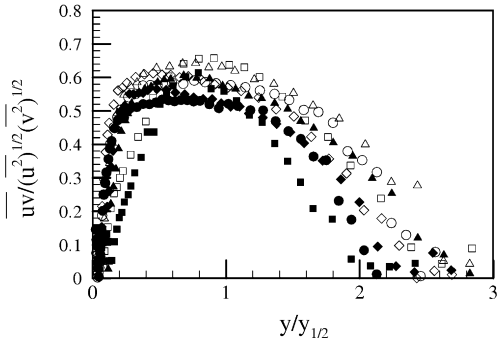

Fig. 6. $\overline{uv}$ correction profiles at different dimensionless circumferential distances, *S/W*: *squares*, 2.79; *triangles*, 4.19; *diamonds*, 5.58; *circles*, 7.74 (*W*=9.38 mm, Re_w=12,000, *Y/W*=9; *filled symbols*, *D/W*=10.7; *hollow symbols*, *D/W*=16)

$\overline{u^2}/U_m^2$ distributions across the wall jet for both semi-cylinders coincide reasonably well at *S/W*=2.79 because their locations are near to the stagnation point, as shown in Fig. 7b. However, the maximum value of $\overline{u^2}/U_m^2$ increases by almost 41% and 50% for 150 mm and 100 mm semi-cylinders respectively when the S/W increases from 2.79 to 7.74. Furthermore, at *S/W*=2.79, the streamwise Reynolds normal stress distributions across the curved wall jet are slightly greater than those of the plane wall jet (i.e. *S/W*= 4.1), as shown in Fig. 5b. However, at nearly the same location of the curved wall jet (*S/W*=4.19), the maximum $\overline{u^2}/U_m^2$ is a factor of 1.29 of that of the plane wall jet, due to the streamwise curvature effect. Though the location at *S/W*=2.79 is very close to the stagnation point, the effect of surface curvature is shown to be significant. As described by Patel and Sotiropouulos (1997), this is due to the effect of surface curvature on the turbulence and, in particular, the Reynolds stresses. With the increase in *S/W* (i.e. *S/W*=7.74), the maximum $\overline{u^2}/U_m^2$ of the curved wall jet is a factor of 1.72 of that of the plane wall jet at *S/W*=4.1.

4.2.2
Slot jet-to-impingement surface distance effect

The initial jet flow characteristics affect the impingement flow along the curved surface. In the wall jet region, the normalised mean velocity profiles at different *Y/W* coincide reasonably well, as shown in Figs. 8a and 9a. In the present study, the maximum $\overline{u^2}/U_m^2$ occurs at *Y/W*=5 and 7 for the surface curvatures, *D/W* of 10.7 and 16 respectively, as shown in Figs. 8b and 9b. The *Y/W* effects can also be found from the radial turbulence intensity and Reynolds shear stress distributions, as shown in Figs. 8c, d and 9c, d.

From the time–mean momentum equations for a two-dimensional turbulent flow over a curved surface as described by Goldstein (1965), a wall jet on a curved surface, especially on a slightly curved surface where $R>>y_m$, the effect of surface curvature on the boundary-layer properties would be very small. However, the present results reveal a considerably larger surface curvature effect than the numerical predictions. Patel and Stotiropoulos (1997) ascribed the difference to the effect of surface curvature on Reynolds stresses in particular. Wilson and Goldstein (1976) described these effects in the production of turbulence energy equations as follows:

$$P_u = -\frac{\overline{u^2}}{1+y/R}\frac{\partial U}{\partial x} - \overline{uv}\frac{\partial U}{\partial y} - \frac{\overline{u^2}V + \overline{uv}U}{R+y} \quad (1)$$

$$P_v = -\frac{\overline{uv}}{1+y/R}\frac{\partial V}{\partial x} - \overline{v^2}\frac{\partial V}{\partial y} + \frac{2\overline{uv}U}{R+y} \quad (2)$$

$$P_{uv} = \frac{\overline{u^2}}{1+y/R}\frac{\partial V}{\partial x} - \overline{v^2}\frac{\partial V}{\partial y} - \frac{\overline{v^2}U}{R+y} + \frac{2\overline{u^2}U}{R+y} \quad (3)$$

The last terms of Eqs. (1) and (2) represent the Coriolis force and centrifugal force contributions to $\overline{u^2}/2$ and $\overline{v^2}/2$ productions respectively. For thin turbulent shear flows where the mean velocity, *V*, in the radial direction is small, the centrifugal force term dominates the P_v and plays an important role for the growth rate of jet thickness due to its curvature effect. Centrifugal force affects the P_u due to the interaction of mean flow and Reynolds stress. This can also be seen from the Reynolds stress production terms in Eq. (3). The third term on the right-hand side in Eq. (3) shows the Coriolis force contribution, while the fourth term represents the centrifugal contribution.

For a slot jet impinging on two different semi-circular convex surfaces, when the location of the dimensionless slot-jet-circumferential distance is small, such as *S/W*=2.79, it is considered to be very close to the reflection region. The mean velocity, *V*, in the radial direction cannot be treated as a small value which plays an important role in $\overline{u^2}/2$ production. During the reflection region, interaction between the air and the cylinder surface is very strong. The increase in flow streamwise turbulent energy production term, P_u, causes a rise in $\overline{u^2}/U_m^2$ in the near-wall region as shown in Figs. 8b and 9b.

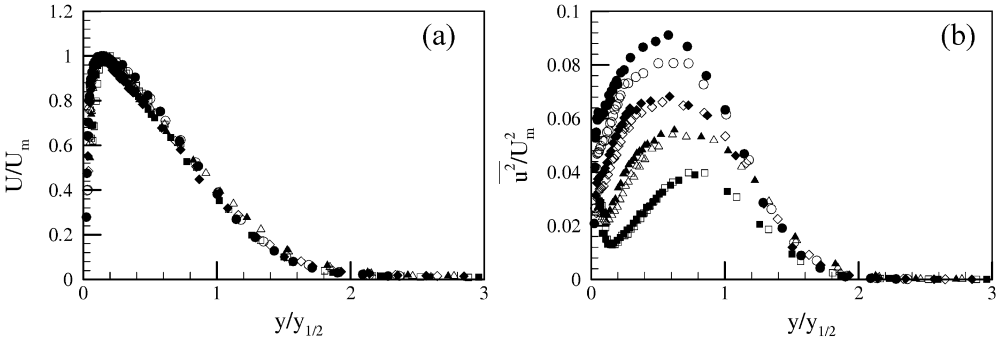

Fig. 7. Effect of surface curvatures on mean velocity and streamwise normal Reynolds stress profiles at different dimensionless circumferential distances, *S/W*: *squares*, 2.79; *triangles*, 4.19; *diamonds*, 5.58; *circles*, 7.74 (*W*=9.38 mm, Re_w=12,000, *Y/W*=7; *filled symbols*, *D/W*=10.7; *hollow symbols*, *D/W*=16)

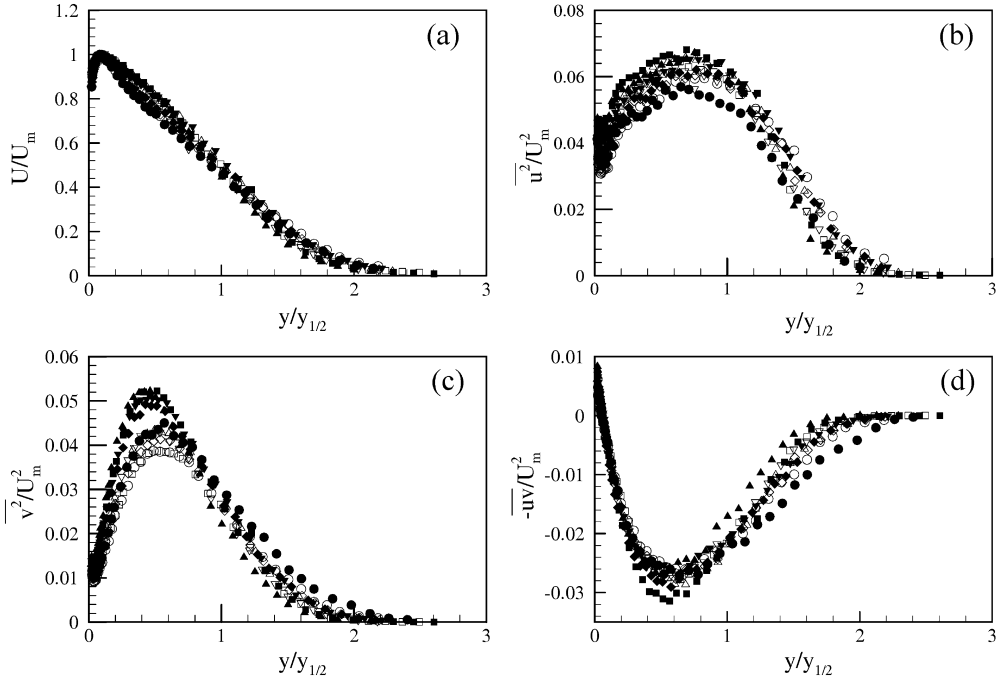

Fig. 8. Effect of surface curvatures on the impingement wall jet flow development at different dimensionless slot jet-to-impingement surface separation distances, *Y/W*: *squares*, 5; *upward triangles*, 7; *downward triangles*, 9; *diamonds*, 11; *circles*, 13 (*W*=9.38 mm, Re_w=12,000, *S/W*=7.74; *filled symbols*, *D/W*=10.7; *hollow symbols*, *D/W*=16)

Figure 10a shows how the ratio of $\sqrt{\overline{u^2}}/\sqrt{\overline{v^2}}$ for the surface curvature effect *D/W*=10.7 and 16 is plotted against $y/y_{1/2}$. Evidently, $\overline{v^2}$ increases due to the surface curvature are apparent near the wall region at $y/y_{1/2}$=0.5. This finding agrees with that of Guitton and Newmann (1977), who studied a two-dimensional wall jet over a logarithmic spiral. In the plane flow, the turbulence energy production term is found only in the equation for $\overline{u^2}$. In the curved flow, however, the equation for $\overline{v^2}$ also contains such a term, as shown in Eq. (2). The turbulence energy production term $\overline{uv}\frac{\partial U}{\partial y}$ appears to be insensitive to curvature within the accuracy of the present measurements, as shown in Fig. 10b. However, the flow structure parameter, $\overline{uv}/q^2$, appears to be sensitive to the surface curvature, as shown in Fig. 10c. In the radial location, from $y/y_{1/2}$=0.25 to 1, $\overline{uv}/q^2$ is slightly increased as the surface curvature increases. However, the dependence of the flow structure parameter, $\overline{uv}/q^2$, on surface curvature is not found along the radial location when $y/y_{1/2}$>1.2.

5 Conclusions

The detailed mean flow and turbulence data of a turbulent air slot jet impinging on two different semi-circular convex surfaces were investigated in both free jet and impingement wall jet regions for the studied jet Reynolds number,

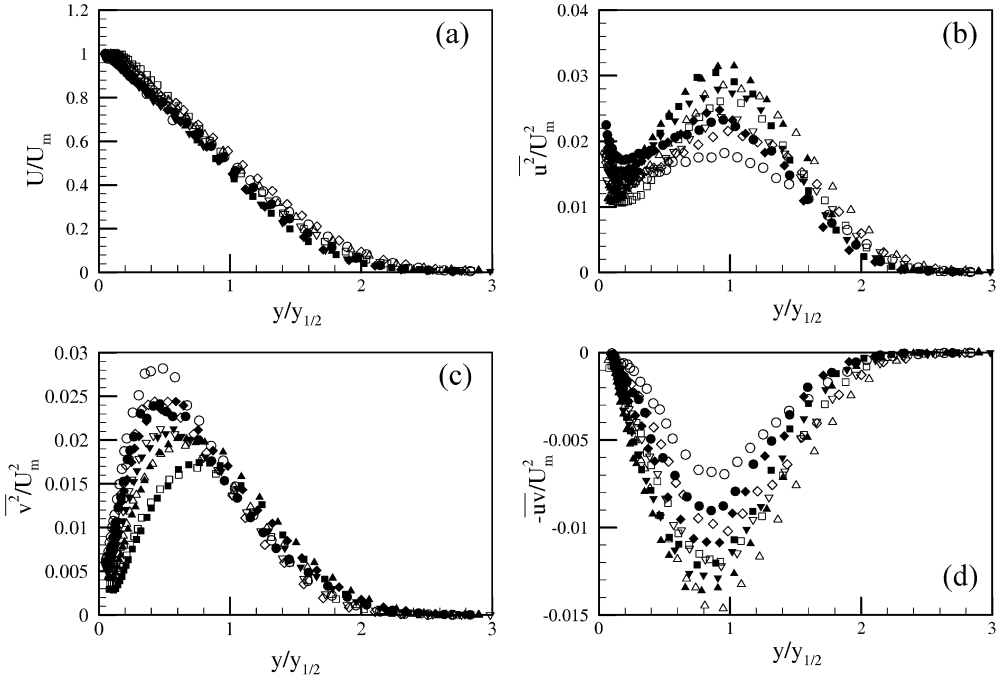

Fig. 9. Effect of surface curvatures on the impingement wall jet flow development at different dimensionless slot jet-to-impingement surface separation distances, *Y/W*: *squares*, 5; *upward triangles*, 7; *downward triangles*, 9; *diamonds*, 11; *circles*, 13 (*W*=9.38 mm, Re_w=12,000, *S/W*=2.79; *filled symbols*, *D/W*=10.7; *hollow symbols*, *D/W*=16)

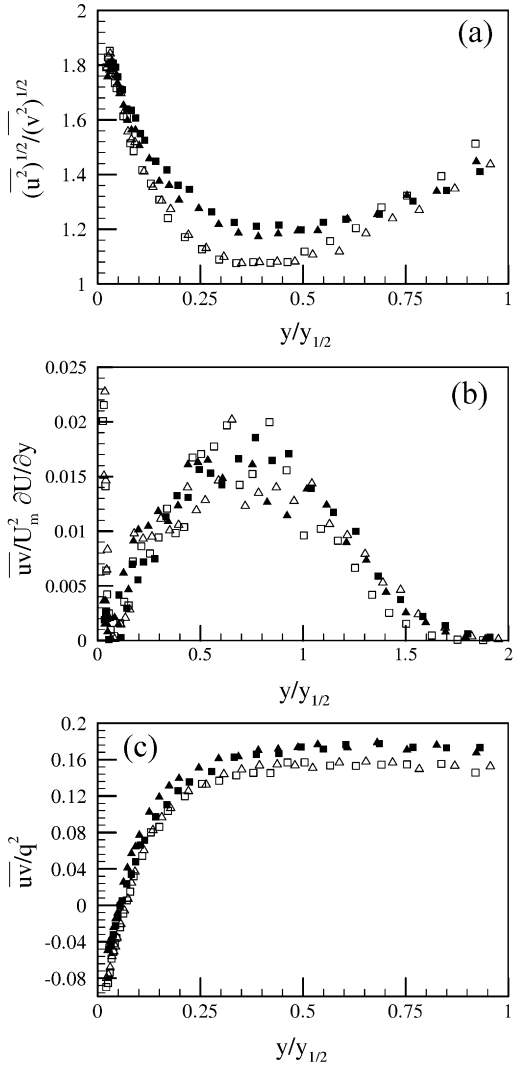

Fig. 10a–c. Effect of surface curvatures on **a** the ratio of $\sqrt{\overline{u^2}}/\sqrt{\overline{v^2}}$, **b** the turbulence production term $\overline{uv}\frac{\partial U}{\partial y}$, and **c** the turbulence structure parameter, $\overline{uv}/\overline{q^2}$ at different dimensionless slot jet-to-impingement surface distances, *Y*/*W*: *squares*, 7; *triangles*, 9 (*W*=9.38 mm, Re_w=12,000, *S*/*W*=7.74; *filled symbols*, *D*/*W*=10.7; *hollow symbols*, *D*/*W*=16)

Re_w=12,000. The parametric effects of dimensionless circumferential distance *S*/*W*, slot jet-to-impingement surface distance *Y*/*W*, and surface curvature *D*/*W* on the impingement wall jet flow development along a semi-circular convex surface were documented into a new set of mean flow and turbulence data for validating and refining turbulence models for future study. The results show that the streamwise and widthwise turbulence intensities, $\overline{u^2}/U_e^2$ and $\overline{v^2}/U_e^2$, along the free jet centreline increase with increasing *Y*/*W* within a certain distance. These findings are useful in helping researchers to understand the heat transfer and turbulence characteristics in stagnation regions of impingement surfaces. The effect of surface curvature *D*/*W* when compared with the results of the curved and plane wall jets is shown to be significant. The results show that the effect of surface curvature *D*/*W* increases with increasing *S*/*W*. Compared with the transverse Reynolds normal stress, $\overline{v^2}/U_m^2$, the streamwise Reynolds normal stresses, $\overline{u^2}/U_m^2$ are strongly affected by the dimensionless parameters of *D*/*W*, *Y*/*W* and *S*/*W* in the near-wall region. It is also found that Reynolds shear stress $-\overline{uv}/U_m^2$ is much more sensitive to the surface curvature, *D*/*W*.

References

Alcaraz E, Charnay G, Mathieu J (1976) Measurements in a wall jet over a convex surface. Phys Fluids 20:203–210

Ashforth-Frost S, Jambunathan K, Whitney CF (1997) Velocity and turbulence characteristics of a semiconfined orthogonally impinging slot jet. Exp Thermal Fluid Sci 14:60–67

Barahma RK, Faruque O, Arora RC (1991) Experimental investigation of mean flow characteristics of slot impingement on a cylinder. Wärme- und Stoffübertragung 26:257–263

Bendat JS, Piersol AG (2000) Random data: analysis and measurement procedures, 3rd edn. John Wiley & Sons Pte Ltd.

Browne LWB, Antonia RA, Chua LP (1989) Calibration of X-probes for turbulent flow measurements. Exp Fluids 7:201–208

Button BL, Leech JR (1972) The selection of a contraction design method, ME Report 395, Lanchester Polytechnic, UK

Chan TL, Jambunathan K, Ashforth-Frost S (1999a) Jet impingement on oblique surface – a bibliography: 1870–1977. Prev Heat Mass Transfer 25:464–473

Chan TL, Jambunathan K, Ashforth-Frost S (1999b) Jet impingement on oblique surface – a bibliography: 1978–1998. Prev Heat Mass Transfer 25:558–570

Chan TL, Leung CW, Jambunathan K, Ashforth-Frost S, Zhou Y, Liu MH (2002) Heat transfer characteristics of slot jet impingement on a semi-circular convex surface. Int J Heat Mass Transfer 45:993–1006

Choi M, Yoo HS, Yang G, Lee JS, Sohn DK (2000) Measurements of impinging jet flow and heat transfer on a semi-circular concave surface. Int J Heat Mass Transfer 43:1811–1822

Downs SJ, James EH (1987) Jet impingement heat transfer – a literature survey. ASME Paper 87-HT-35

Faruque O, Brahma RK, Arora RC (1992) Flow characteristics of slot jet impingement on a wedge. Warme- und Stoffubertragung 27:421-427.

Fujisawa N, Kobayashi R (1987) Turbulence characteristics of wall jets along strong convex surfaces. Int J Mech Sci 29:311–320

Gardon R, Akfirat JC (1965) The role of turbulence in determining the heat characteristics of impinging jets. Int J Heat Mass Transfer 8:1261–1272

Gau C, Chung CM (1991) Surface curvature effect on slot–air-jet impingement cooling flow and heat transfer process. ASME J Heat Transfer 113:858–864

Gibson MM, Verriopoulos CA, Vlachos NS (1984) Turbulent boundary layer on a mildly curved convex surface. 1. Mean flow and turbulence measurements. Exp Fluids 2:17–24

Goldstein S (1965) Modern developments in fluid dynamics, vol 1. Dover, New York

Guitton DE, Newmann BG (1977) Self-preserving turbulent wall jets over convex surfaces. J Fluid Mech 8:155–185

Hrycak P (1981) Heat transfer from impinging jets – a literature review. AFWAL-TR-81-3054, June 1981, Air Force Wright Aeronautical Laboratories, Ohio, USA, 63 pp

Holman JP (1978) Experimental methods for engineers, 3rd edn. McGraw-Hill, New York

Jambunathan K, Lai E, Moss MA, Button BL (1992) A review of heat transfer data for single circular jet impingement. Int J Heat Fluid Flow 13:106–115

Kobayashi R, Fujisawa N (1983) Curvature effects on two-dimensional turbulent wall jets along concave surfaces. Bull JSME 26: 2074–2080

Launder BE, Rodi W (1981) The turbulent wall jet. Prog Aerospace Sci 19:81–128

Lee DH, Chung YS, Kim DS (1997) Turbulent flow and heat transfer measurements on a curved surface with a fully developed round impinging jet. Int J Heat Fluid Flow 18:160–169

Liu MH, Chan TL, Zhou Y, Leung CW (2000) A turbulent slot jet impinging on a semi-cylindrical convex surface. In: Bu-Xuan Wang (ed) Proc of the 5th Int Symp on Heat Transfer, Beijing,

12–16 August, in Heat Transfer Science and Technology. Higher Education Press, Beijing, pp 655–660
Livingood JNB, Hrycak P (1973) Impingement heat transfer from turbulent air jets to flat plates – a literature survey. NASA TM X-2778, May 1973, 43pp.
Martin H (1977) Heat and mass transfer between impinging gas jets and solid surfaces. Adv Heat Transfer 13:1–60
Neuendorf R, Wygnanski I (1999) On a turbulent wall jet flowing over a circular cylinder. J Fluid Mech 381:1–25
Patel VC, Sotiropoulos F (1997) Longitudinal curvature effects in turbulent boundary layers. Prog Aerospace Sci 33:1–70
Piquet J, Patel VC (1999) Transverse curvature effects in turbulent boundary layer. Prog Aerospace Sci 35:661–672
Talamelli A, Westin KJA, Alfredsson PH (2000) An experimental investigation of the response of hot-wire x-probes in shear flows. Exp Fluids 28:425–435
Vickers JMF (1959) Heat transfer coefficients between fluid jets and normal surfaces. Ind Eng Chem 51:967–972
Viskanta R (1993) Heat transfer to impinging isothermal gas and flame jets. Exp Thermal Fluid Sci 6:111–134
Wilson DJ, Goldstein RJ (1976) Turbulent wall jets with cylindrical streamwise surface curvature. ASME J Fluids Eng 98:550–556
Yamada H, Nakamura I, Yamashita S, Yano H (1990) Experiments on a two-dimensional impinging jet on a wedge (turbulence properties and the energy balance), JSME Int J, Series II, 33: 80-87.
Yang G, Choi M, Lee JS (1999) An experimental study of slot jet impingement cooling on concave surface: effects of nozzle configuration and curvature. Int J Heat Mass Transfer 42:2199–2209
Zhou Y, So RMC, Liu MH, Zhang HJ (2000) Complex turbulent wakes generated by two and three side-by-side cylinders. Int J Heat Fluid Flow 21:125–133